nature water

Article

https://doi.org/10.1038/s44221-023-00113-5

Shielding effect enables fast ion transfer through nanoporous membrane for highly energy-efficient electrodialysis

In the format provided by the authors and unedited

Supplementary Materials for

Shielding effect enables fast ion transfer through nanoporous membrane for highly energy-efficient electrodialysis

This PDF file includes:

1. Supplementary methods

1.1. Materials and chemicals

Five commercial anion exchange membranes (AEMs), i.e., AEM-1, AEM-2, AEM-3, AEM-4 and AEM-5, were obtained for comparison of desalination performance with the PDA/PEI-coated TFC NPMs. Specifically, AEM-1 was supplied from Guangdong Yinachuan Environmental Technology Co., Ltd. (China). AEM-2 was supplied from Shandong Tianwei Membrane Technology Co., Ltd. (China). AEM-3 and AEM-4 were kindly supplied from Fumatech (Germany). AEM-5 were supplied from ASTOM (Japan). The properties of these commercial AEMs are shown in **Table S1**.

1.2 Membrane characterization

1.2.1 Thickness of selective layer of the TFC NPMs

An atomic force microscope (AFM, Agilent 5500, USA) was used to accurately measure the thickness of the selective layer of the TFC NPMs (1, 2). Prior to the AFM measurement, the selective polyamide layer was peeled-off from the polysulfone (PS) substrate using scotch tape, tweezers, and *N*, *N*-dimethylformamide (DMAc) solvent. It was then transferred onto a silicon wafer to make "polyamide (PA) film-silicon wafer" sample. The process involves several steps: (i) the PA layer side of the NPMs was first taped using scotch tape. Then, the nonwoven fabric attached into the PS substrate was stripped with the tweezers to obtain the PA/PS substrate adhered to the tape, (ii) the PA/PS substrate composite was immersed in the methanol solvent to release it from the scotch tape, (iii) the PA/PS substrate composite was immersed in DMAc solvent to remove the PS substrate and an isolated PA film was consequently obtained, and (iv) the isolated PA film was then transferred to the silicon wafer, which was washed with DMAc and methanol solvent. The "PA film-silicon wafer" sample was prepared after drying in air. Furthermore, a scratch on the PA film was created with a sharp scalpel, so the location of the cross-section between the PA film and silicon wafer was found and detected by an AFM probe during the measurement. The gap between the silicon wafer surface and the PA film was considered to be the thickness of the PA layer. The AFM images were processed using Gwyddion 2.48 software.

1.2.2 Specific areal electric resistance of the TFC NPMs

A membrane resistance analysis cell (ChemJoy Polymer Material Co., Ltd., China) was custom-designed to measure the specific areal resistance of the anion conduction membranes (ACMs) before and after the electrodialysis (including PDA/PEI-coated TFC NPMs and conventional AEMs) in the standard measurement condition using a 0.5 $mol \cdot L^{-1}$ NaCl solution at 25°C (3). The measurement cell was composed of four compartments, which are made of Perspex sheets. Each compartment was isolated by cation exchange membranes (CEMs) or ACMs with an effective area of 7.065 cm^2. The titanium plates coated with iridium oxide and tantalum oxide were applied as the cathode and anode, respectively. Furthermore, the toroid gaskets were placed between each compartment to ensure the sealing of the measurement cell. The commercial CEM (CJMC-3, ChemJoy Polymer Material Co., Ltd., China) was employed as an auxiliary membrane and was inserted between the electrodes (cathode and anode) and the tested ACMs (PDA/PEI-coated TFC NPMs and commercial AEMs), which can effectively isolate the tested NaCl solution (0.5 $mol \cdot L^{-1}$) and the Na_2SO_4 electrolyte solution (0.3 $mol \cdot L^{-1}$). The specific areal electric resistance of the ACMs was measured at a fixed current of 0.1 A, as calculated using Eq. S1 (4):

$$R_A = \frac{U - U_0}{I} \cdot S \quad \text{(S1)}$$

Here, U is the trans-membrane voltage, U_0 is the blank voltage without ACM tests, I is the constant current applied in the measurement cell (i.e., 0.1 A), and S is the effective area of the tested ACMs (i.e., 7.065 cm^2). The specific areal resistance measurement of the ACMs was not conducted during the electrodialysis test. Since the concentration of NaCl in both concentrate and diluate chambers changes due to the ion transfer under the electric field, the electric resistance of the ACMs changes as well. Therefore, the specific areal resistance of the ACMs was measured after the test in the 0.5 $mol \cdot L^{-1}$ NaCl solution at 25 °C in this case.

1.2.3 Pore size and molecular weight cut-off of the TFC NPMs

The separation of 0.2 $g \cdot L^{-1}$ poly(ethylene glycol) (PEG) solutions (molecular weights (MW) of 200, 300, 400, 600 and 1000 Da, respectively) were performed at 4 bar to determine the pore size of the NPMs. Due to their low MWs, the PEGs were assumed to be spherical. The correlation between the Stokes diameter (d_s) of the PEGs and their MW can be expressed by Eq. S2 (5, 6):

$$d_s = 33.46 \times 10^{-12} \times MW^{0.557} \quad \text{(S2)}$$

After the filtration of the PEG solutions at 4 bar, the concentration of the polyethylene glycol polymers in the feed (C_f) and permeate (C_p) were measured using a total organic carbon analyzer (TOC-L CpH/CPN, Shimadzu Corporation, Japan) with the oxidizing combustion-infrared analysis method. The rejection (R) of the PEGs for the TFC NPMs was calculated using Eq. S3:

$$R = \frac{C_f - C_p}{C_f} \quad \text{(S3)}$$

Afterwards, a log-normal probability density function between the Stokes diameter (d_p) of the PEGs and their rejection coefficients (R) was employed to quantify the membrane pore size distribution, as displayed in Eq. S4 (5-8):

$$\frac{dR(d_p)}{d(d_p)} = \frac{1}{d_p \ln\sigma_p \sqrt{2\pi}} \exp\left[-\frac{\left(\ln d_p - \ln\mu_p\right)^2}{2\left(\ln\sigma_p\right)^2} \right] \quad \text{(S4)}$$

Here, μ_p denotes the mean effective pore size of the NPMs, which is determined at R of 50%. σ_p is the geometric standard deviation for pore size, which is defined as the ratio of the pore size determined at the R value of 84.13% to μ_p.

Furthermore, the molecular weight cut-off (MWCO) of the TFC NPMs was back-calculated based on the solute Stokes diameter at the R value of 90% using Eq. S2.

1.2.4 Molecular dynamics simulation

Molecular dynamics (MD) simulation was performed to investigate the mass transfer of the PDA/PEI-coated TFC NPMs in electrodialysis. To ensure reasonable computational limits, the MD simulation was limited to the interaction surface area for the NPM, which is highlighted in the red box in **Fig. 4E**. A periodic boundary condition (PBC) was implemented on all sides of the

domain to allow the simulated molecules to flow in a manner consistent with the experiment. However, salt ions were allowed to leave and reenter the domain due to the implementation of the PBC. The MD simulation domain was designed to study the interactions of the salt ions and organic molecule with the PDA/PEI-coated TFC NPMs under the influence of an electric field. The domain included a molecular model of the PDA/PEI complex layer that makes up the coating on the NPMs. The domain was then solvated with water molecules at a density of 1 $g \cdot cm^{-3}$. Sufficient salt ions (Na^+ and Cl^- ions) were added based on a salinity of 12 $g \cdot L^{-1}$, consistent with experiments. In addition, an ampicillin sodium molecule was added to the salt (NaCl) solution so that the molecular scale movements of ampicillin ions around the PDA/PEI complex layer could be investigated.

First, the molecular model of the PDA/PEI complex layer was built. Various PDA/PEI formulations gave rise to different net charges. As indicated in the zeta potential measurements (**Fig. 1F**), the PDA/PEI complex layer possessed a slightly negative net charge. Based on this, the PDA/PEI complex structure was built using Materials Studio by first sketching a short chain unit of PEI monomer and replacing selected N atoms from PEI monomer with the N atom of dopamine molecules as demonstrated by the Schiff-base reaction. The structures of both PEI monomer and dopamine molecule were built with references from the PubChem database (9, 10).

Various structures with different ratios of PDA/PEI complexes were obtained using BIOVIA Materials Studio Forcite software, where molecular mechanics were applied to optimize the molecular geometry using the Universal Force Field (UFF). Thereafter, the partial charge of the PDA/PEI complexes was extracted by converting the PDB file exported from Materials Studio into a CSSR format using the open-source chemistry toolbox software Open Babel (11).

Based on a thorough investigation, we found that the configuration where N atoms from PEI monomer were replaced with the dopamine dimer most closely resembled what was experimentally formulated. The dopamine dimer was formed based on covalent polymerization between two single dopamine molecules. For every 4 PEI monomers, 3 H atoms that are attached to an N atom would be replaced with a PEI branch, which were then each attached to the dopamine dimer. It was found that this repeating unit provides a net charge of -0.036*e*, consistent with zeta potential measurement (**Fig. 1F**). The MD simulation used the 30 repeating units as the PDA/PEI complex.

In addition, ampicillin sodium (whose molecular structure was obtained from PubChem (12)) was imported into Materials Studio Forcite to remove the Na^+ ion, prior to geometry optimization using UFF. This created a negatively charged ampicillin ion with charge of -3. The partial charge distribution was obtained via Open Babel (11).

Based on the molecular structure of the PDA/PEI complex and ampicillin ion, Moltemplate (13) was used to construct the domain as seen in **Fig. 4E**. The general amber force field (GAFF) (14) was employed to model the intra- and inter-molecular interactions between the PDA/PEI complex and ampicillin ion. Water molecules were modelled using the TIP3P model (15) with a long-range Coulombic solver. The particle-particle particle-mesh solver (PPPM) long-range Coulombic solver was employed in this study. The interactions of monovalent salt ion were modelled based on Lennard-Jones interactions with Coulombic potential whose parameters were obtained from

Joung et al. (16). The inter-molecular interactions between the PDA/PEI complex and ampicillin ion were modelled using the mixing rule for the Lennard-Jones interactions. The global cutoff distances for Lennard-Jones and Coulombic forces were specified to be 9 Å and 10 Å, respectively. In this study, the Large-scale Atomic/Molecular Massively Parallel Simulator (LAMMPS) (17) was used for all MD simulations, and the visualizations were performed using Visual Molecular Dynamics (18).

From the initial configuration shown in Error! Reference source not found.**4E**, all atoms were given a random drift velocity at a temperature of 300 K. The system was then minimized using a conjugate gradient algorithm. Afterwards, the PDA/PEI complex layer was held frozen, while the water molecules, ampicillin ions and salt ions were allowed to equilibrate at canonical NVT ensemble for 0.05 ns at a time step of 1 fs. Subsequently, the PDA/PEI complex layer was unfrozen with its N atoms constrained in the axial direction. This would emulate the bond of the PDA/PEI complex layer on the TFC NPM substrate. The entire system was then subjected to equilibration in NVT conditions for 15 ns. Finally, an electric field of magnitude of 1×10^{-2} V/Å was applied across the simulation domain. Although we calculated that the electric field applied is closer to 5×10^{-5} V/Å in the experiment, a larger electric field is required in MD simulations so that the interaction can be observed in a reasonable computational time. Such a MD technique has been applied in the elucidating the mass transport of permeable membranes (19, 20). The simulation run was repeated three times, and the drift velocity of Cl^-, Na^+ and ampicillin ions was averaged over time for 15 ns, as shown in **Fig. 4F**.

2. Supplementary data and figures

2.1 Characterization of the PDA/PEI-coated NPMs

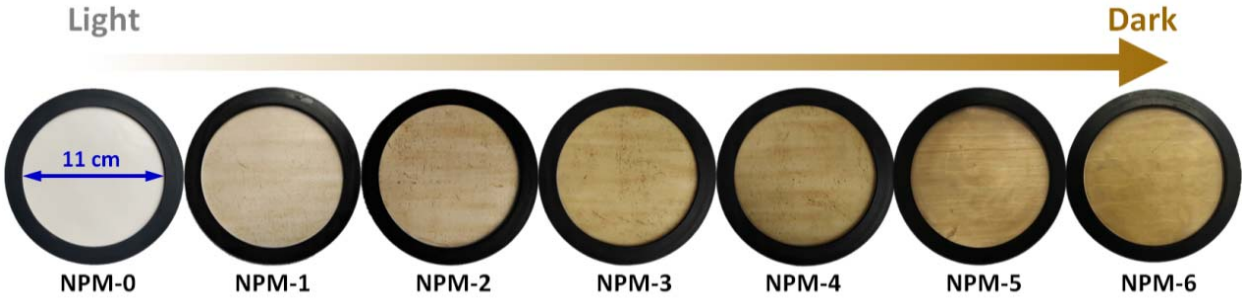

Fig. S1. Photographs of surface color pattern for the PDA/PEI-coated NPMs via co-deposition of dopamine and PEI at different coating durations.

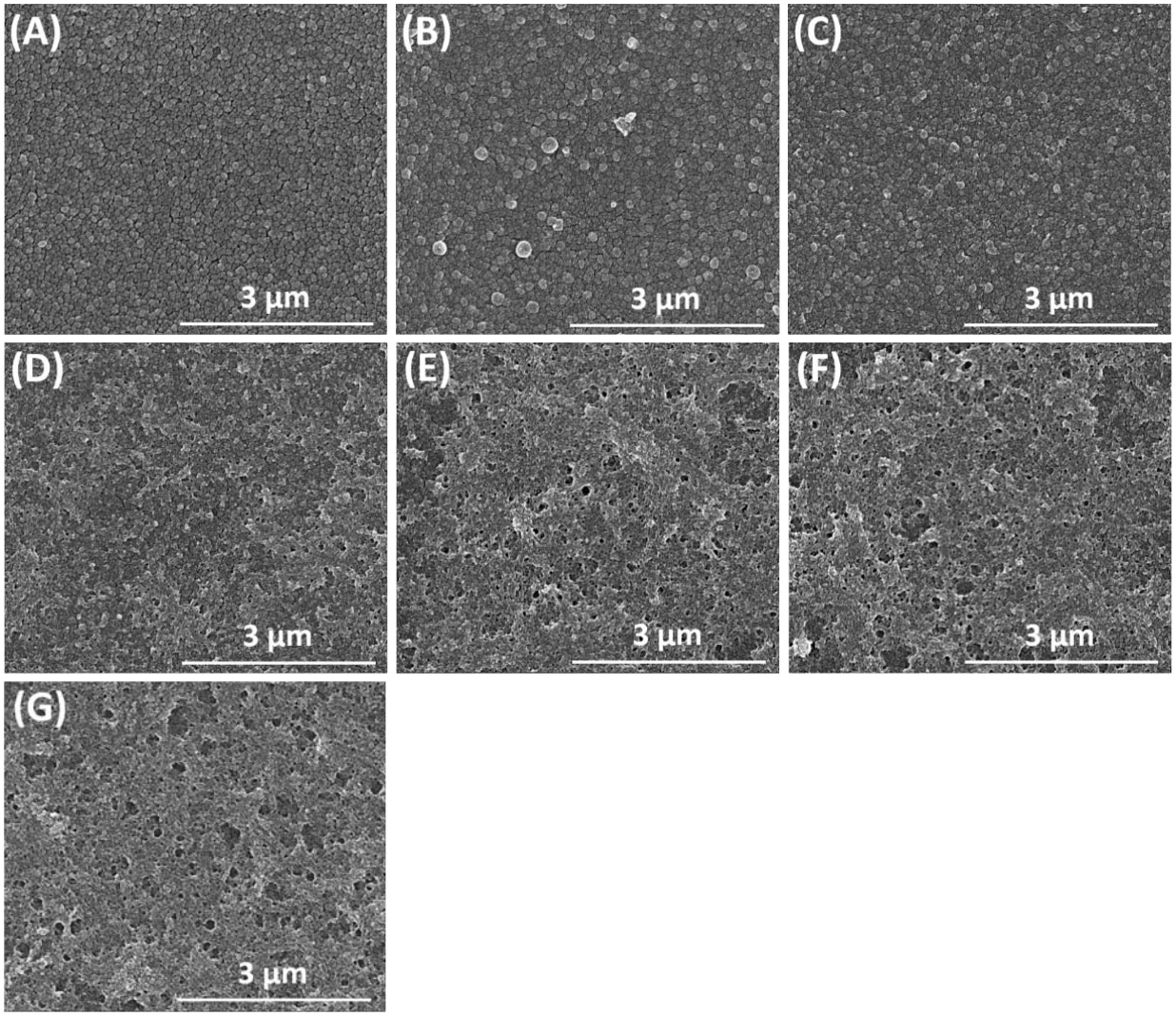

Fig. S2. Surface morphologies of the TFC NPMs before and after the mussel-inspired PDA/PEI coating: (**A**) NPM-0, (**B**) NPM-1, (**C**) NPM-2, (**D**) NPM-3, (**E**) NPM-4, (**F**) NPM-5, and (**G**) NPM-6.

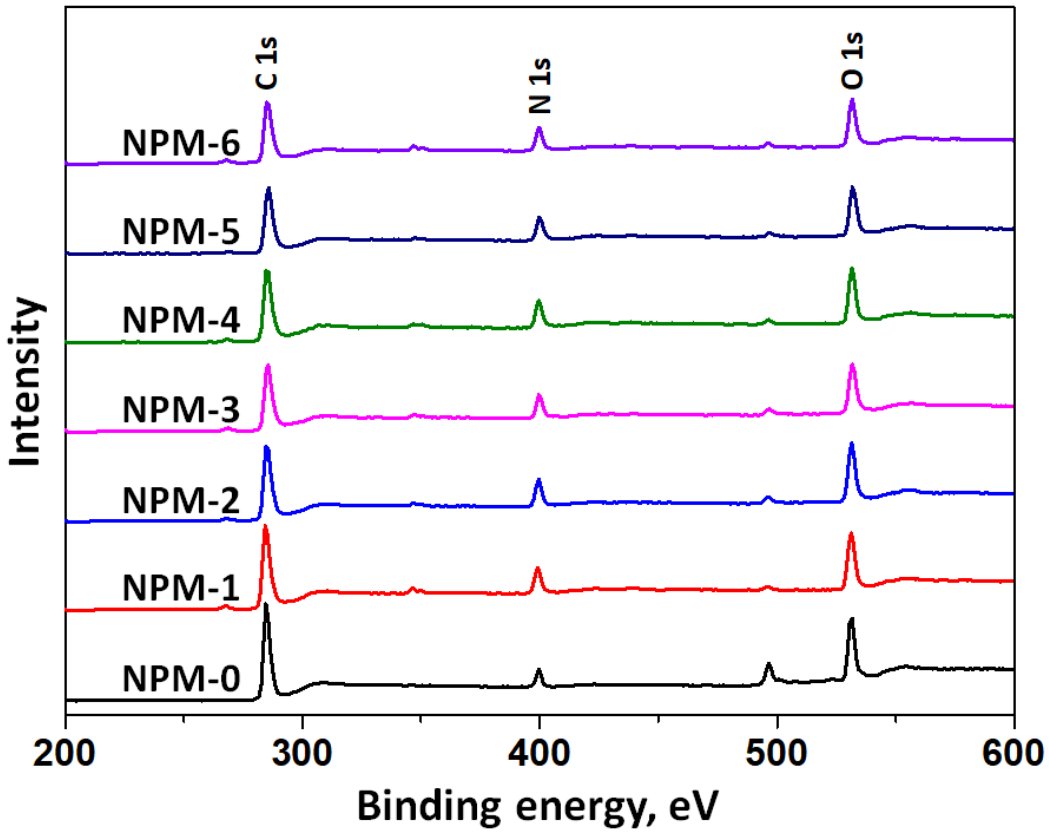

Fig. S3. XPS survey spectra of the PDA/PEI-coated NPMs.

As demonstrated in **Fig. S3**, the pristine loose NPM substrate and the PDA/PEI-coated NPMs exhibited identical elemental peaks including carbon (C 1s), nitrogen (N 1s) and oxygen (O 1s) in the XPS spectra. However, compared to the pristine loose NPM substrate, the PDA/PEI-coated NPMs showed an increasing intensity of the N 1s peak and a decrease in the intensity of the C 1s peak, suggesting the effective co-deposition of the PDA/PEI complex on the membrane surface. Specifically, the presence of N groups increased from 6.5% (NPM-0) to 12.6% (NPM-6) (**Table S2**) due to the intercalation of PEI molecules with a higher atomic percentage of N in the membrane surface through Schiff base or/and Michael addition reactions with dopamine (21-24).

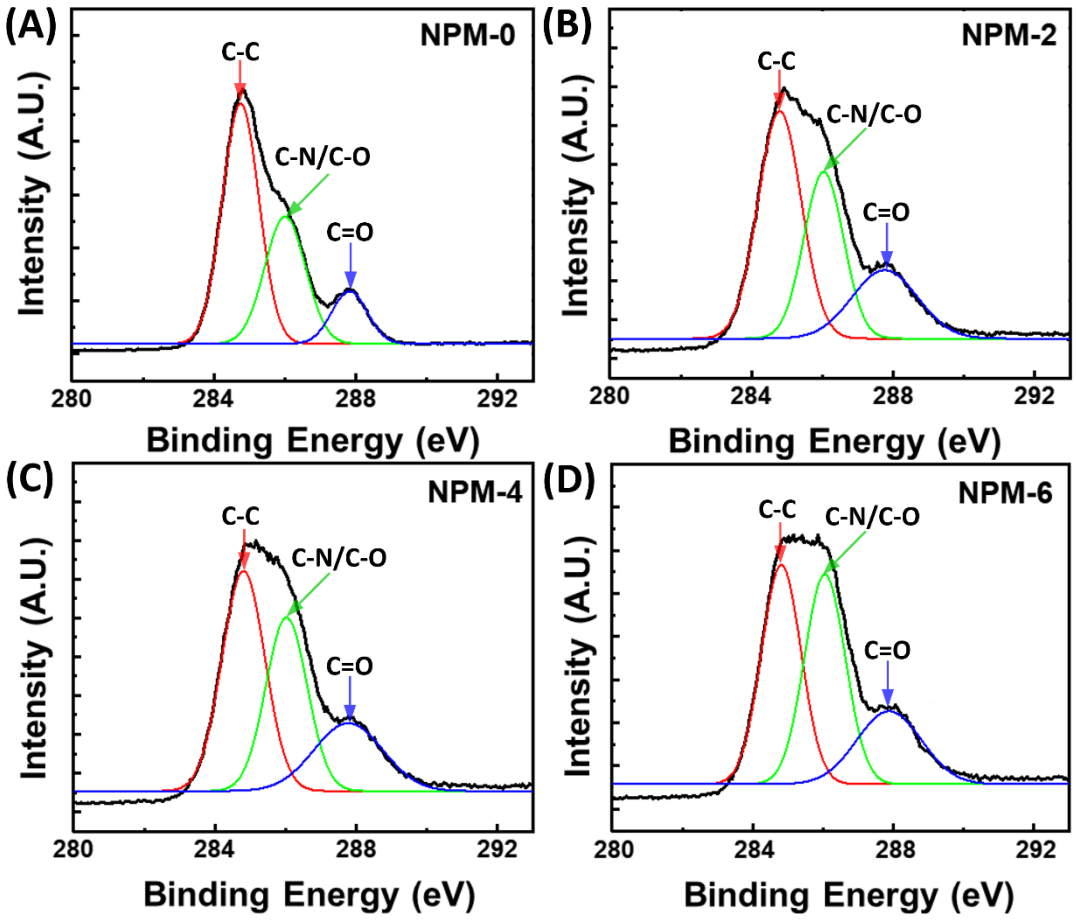

Fig. S4. High-resolution XPS spectra for C1s of the pristine (NPM-0) and PDA/PEI-coated NPMs (NPM-2, NPM-4 and NPM-6).

XPS C1s spectra of (A) NPM-0, (B) NPM-2, (C) NPM-4, (D) NPM-6. PDA/PEI-coated NPMs exhibits an increase in intensity of C-N/C-O (at the peak of 286.5 eV) and C=O (at the peak of 287.8 eV) bonding, compared to the pristine loose nanofiltration membrane substrate (NPM-0), indicating the occurrence of Schiff base and/or Michael addition between dopamine and PEI onto the pristine loose nanofiltration membrane substrate (NPM-0). Furthermore, it also confirms the degree of binding between dopamine and PEI and the bridging between the resultant PDA/PEI complex and loose nanofiltration membrane substrate (NPM-0) as co-deposition coating duration increases.

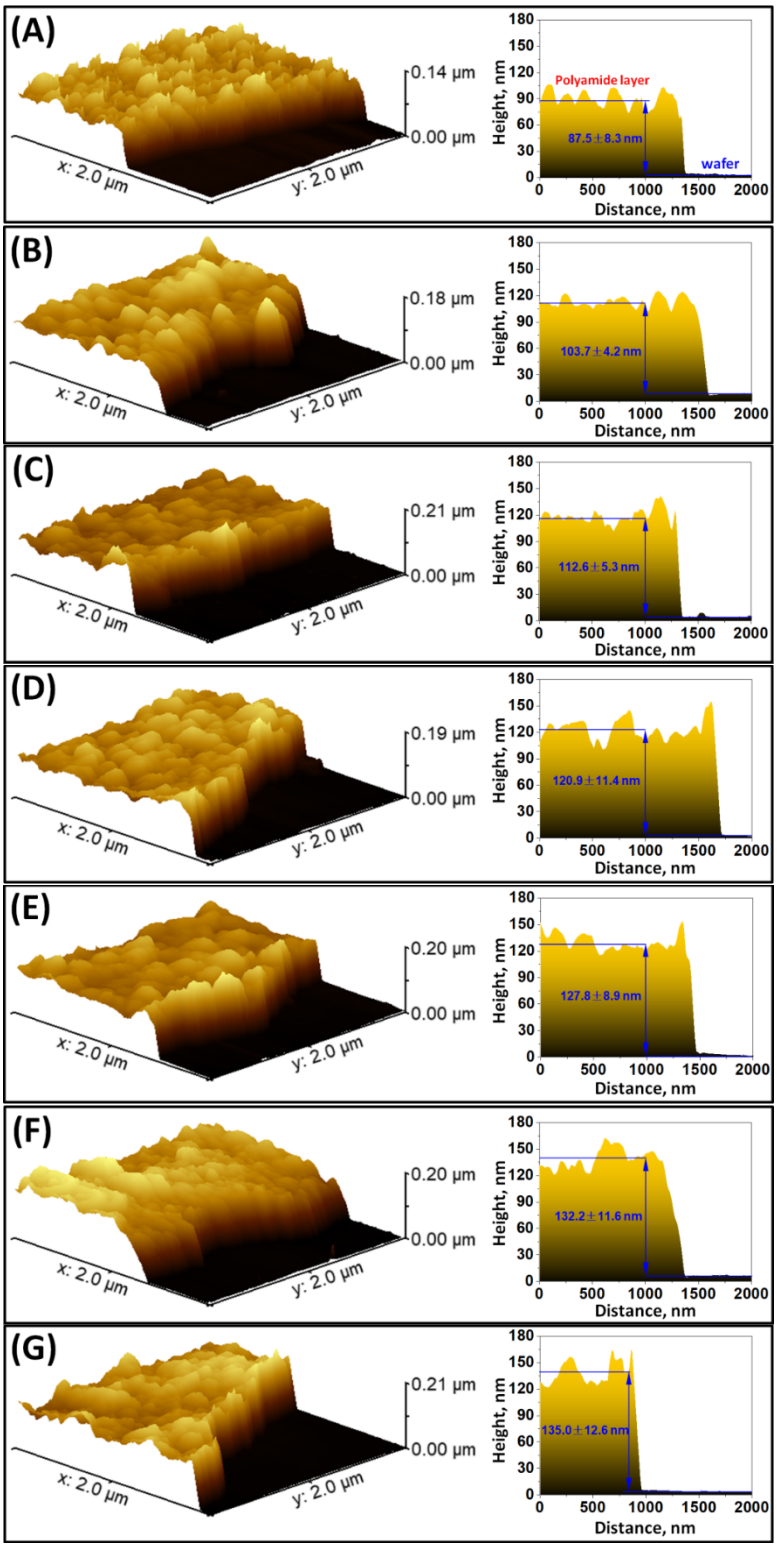

Fig. S5. AFM surface topography and thickness variation of the selective layer of the PDA/PEI-coated TFC NPMs: (**A**) NPM-0, (**B**) NPM-1, (**C**) NPM-2, (**D**) NPM-3, (**E**) NPM-4, (**F**) NPM-5, and (**G**) NPM-6.

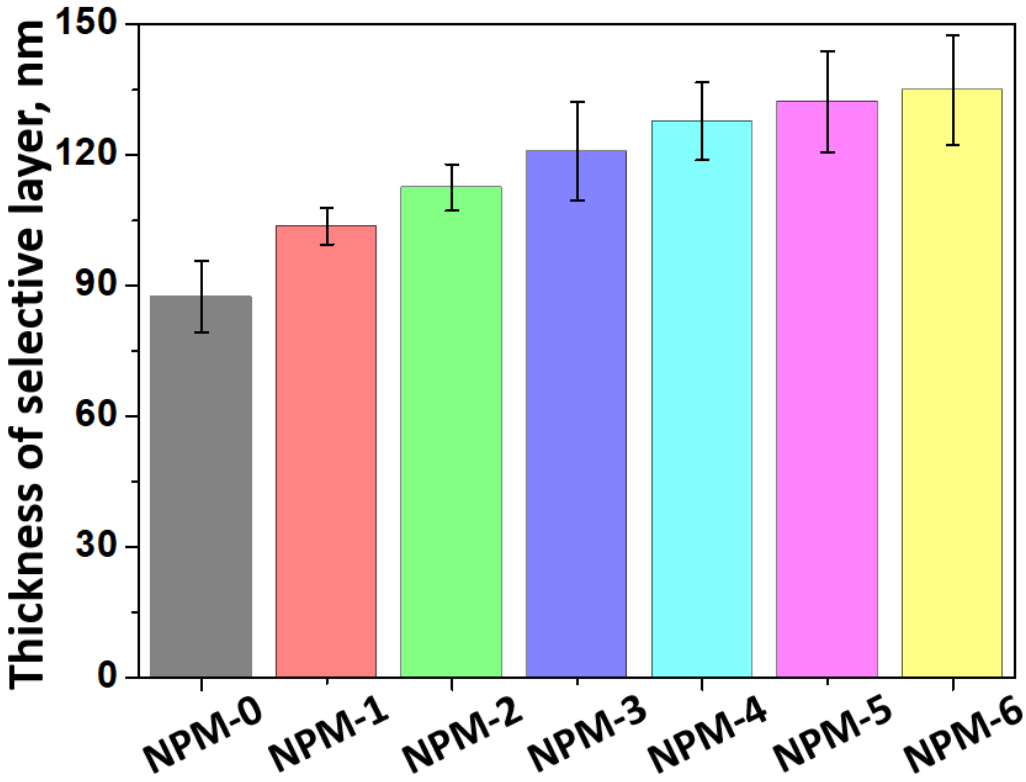

Fig. S6. Evolution in selective layer thickness of the NPMs after bioinspired coating of PDA/PEI complex layer at different coating durations.

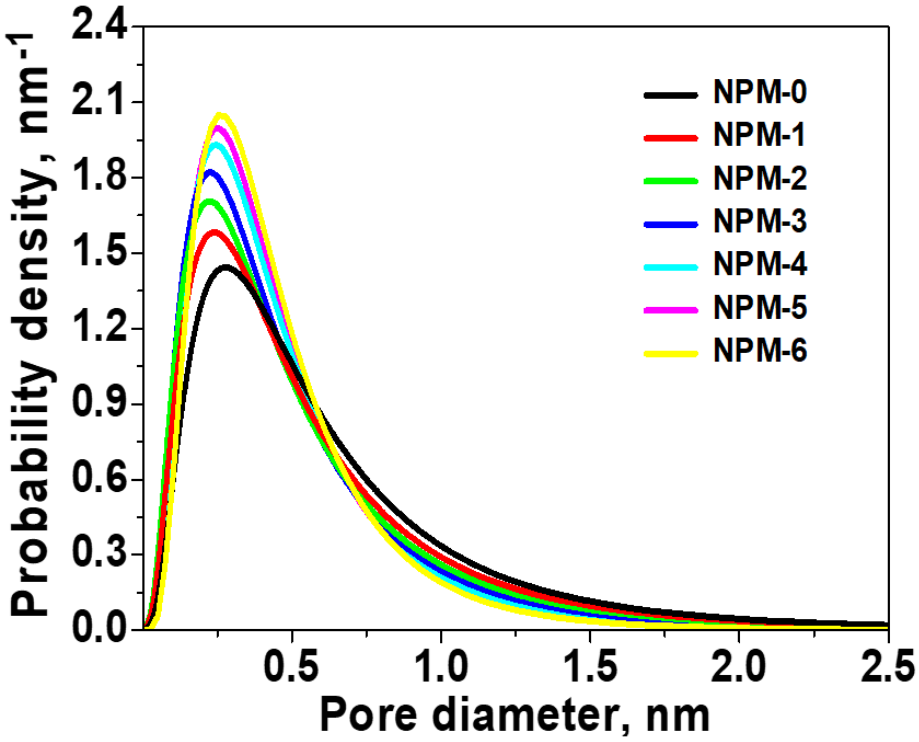

Fig. S7. Calculated pore size distribution of the PDA/PEI-coated TFC NPMs.

2.2 Pressure-driven separation performance of PDA/PEI-coated TFC NPMs

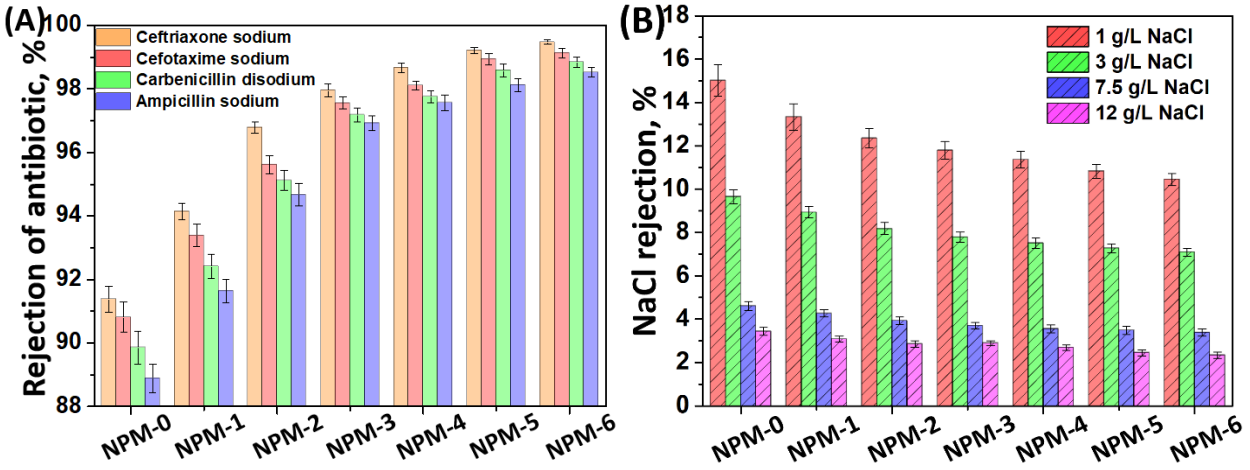

Fig. S8. Individual rejection of antibiotics and NaCl for the PDA/EPI-coated TFC NPMs in a pressure-driven filtration: (**A**) Antibiotics only and (**B**) NaCl only.

2.3 Pressure-driven constant-volume nanofiltration-based diafiltration using NPM-6 membrane for fractionation of antibiotics and NaCl

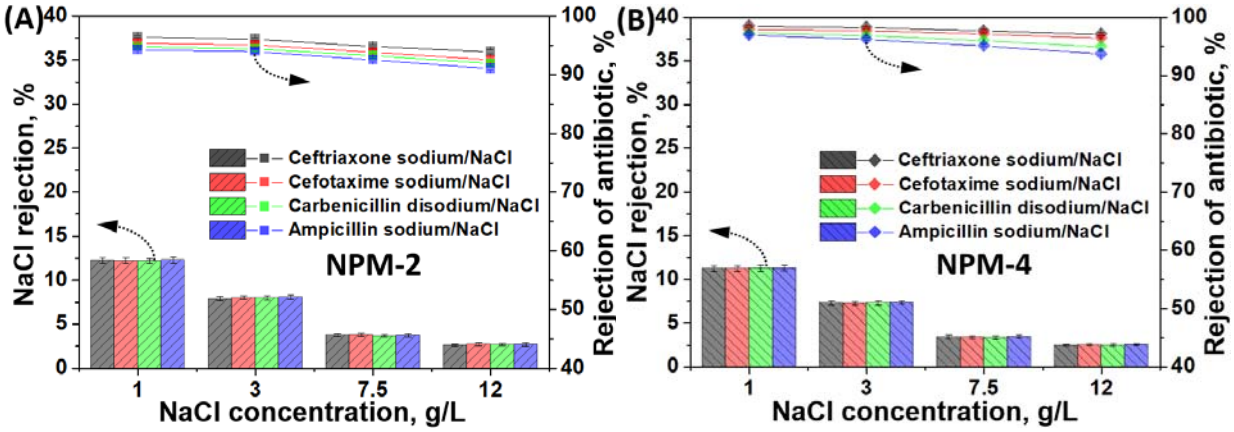

Fig. S9. Rejection of antibiotics and NaCl for the NPM membranes when filtering various antibiotic/NaCl mixed solutions: (**A**) NPM-2 and (**B**) NPM-4.

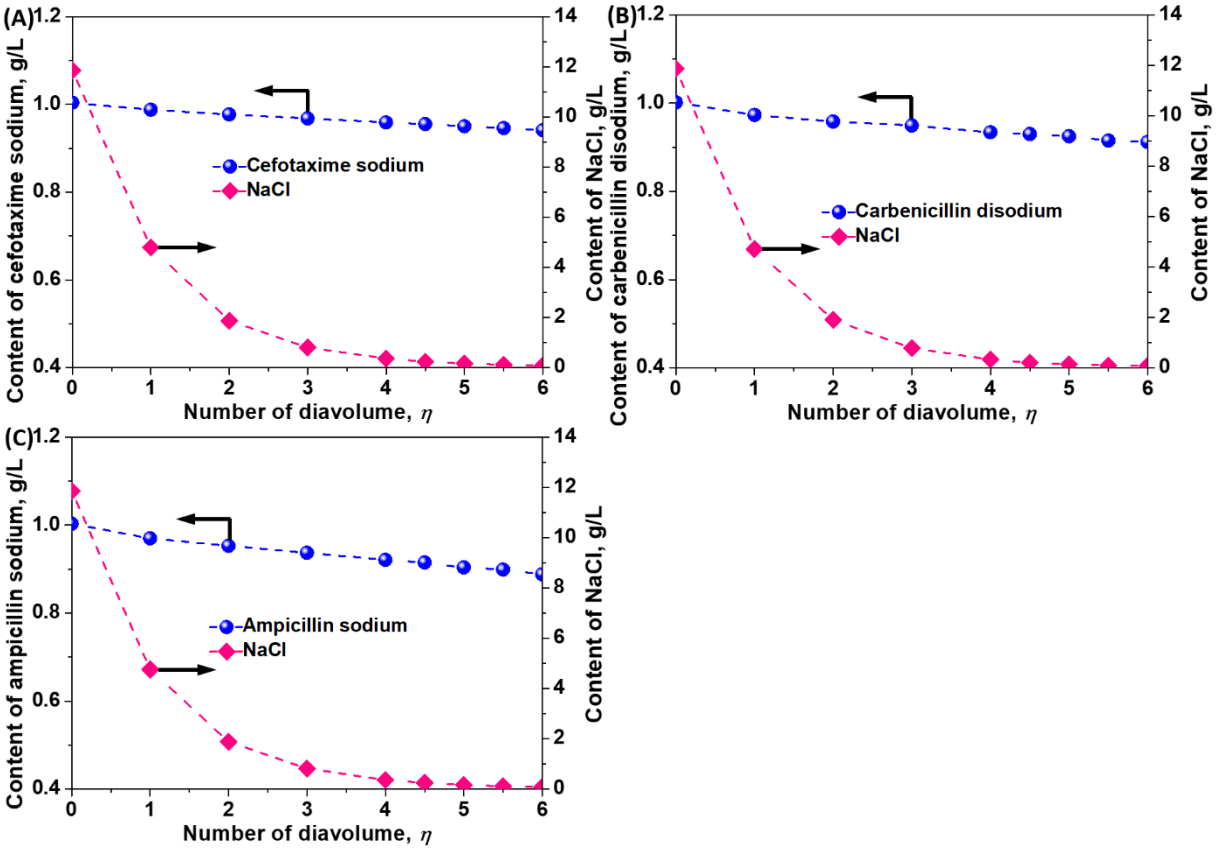

Fig. S10. Content of antibiotic and NaCl in the feed during the constant-volume nanofiltration-based diafiltration using the NPM-6 membrane for fractionation of antibiotics and NaCl from antibiotics/NaCl mixed solutions. (**A**) Cefotaxime sodium/NaCl, (**B**) carbenicillin disodium/NaCl, and (**C**) ampicillin sodium/NaCl mixed solution.

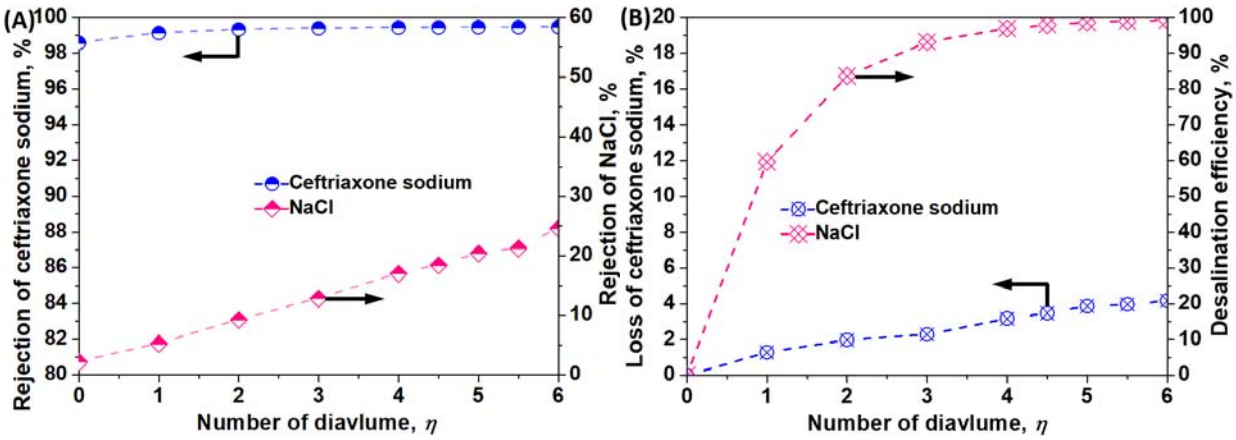

Fig. S11. Pressure-driven constant-volume nanofiltration-diafiltration performance of the NPM-6 membrane for fractionation of ceftriaxone sodium and NaCl from the ceftriaxone sodium/NaCl mixed solution. (**A**) Rejection of ceftriaxone sodium and NaCl and (**B**) loss of ceftriaxone sodium and desalination efficiency.

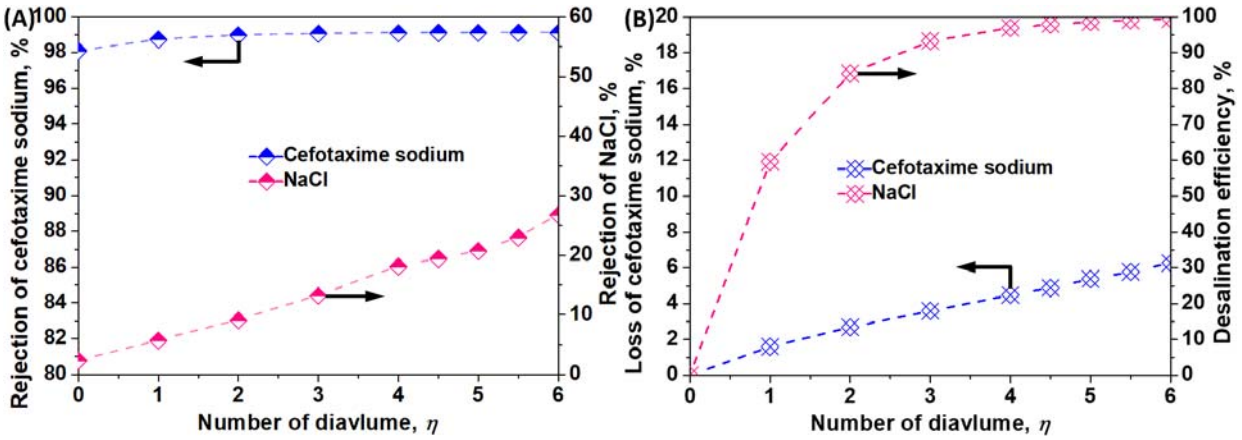

Fig. S12. Pressure-driven constant-volume nanofiltration-diafiltration performance of the NPM-6 membrane for fractionation of cefotaxime sodium and NaCl from the cefotaxime sodium/NaCl mixed solution. (**A**) Rejection of cefotaxime sodium and NaCl and (**B**) loss of cefotaxime sodium and desalination efficiency.

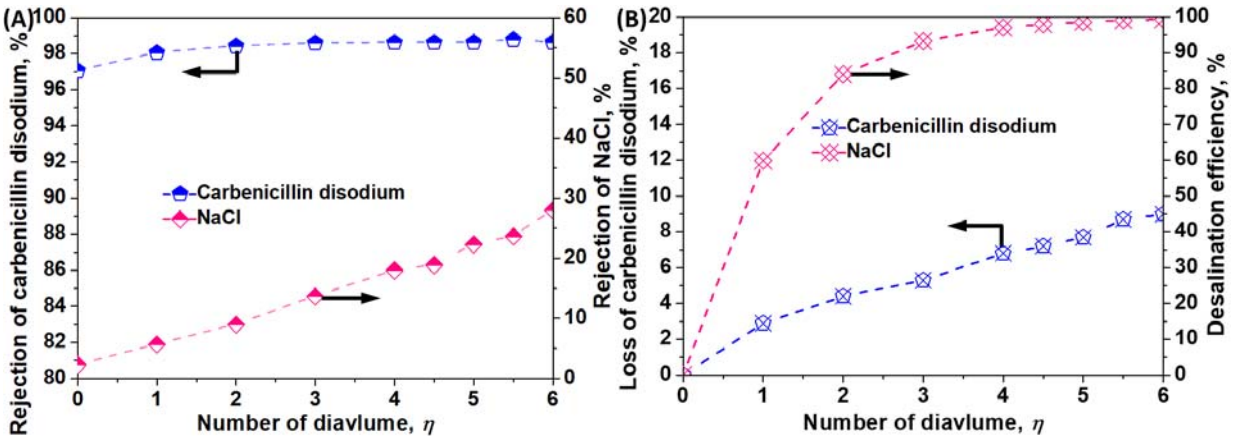

Fig. S13. Pressure-driven constant-volume nanofiltration-diafiltration performance of the NPM-6 membrane for fractionation of carbenicillin disodium and NaCl from the carbenicillin disodium/NaCl mixed solution. (**A**) Rejection of carbenicillin disodium and NaCl and (**B**) loss of carbenicillin disodium and desalination efficiency.

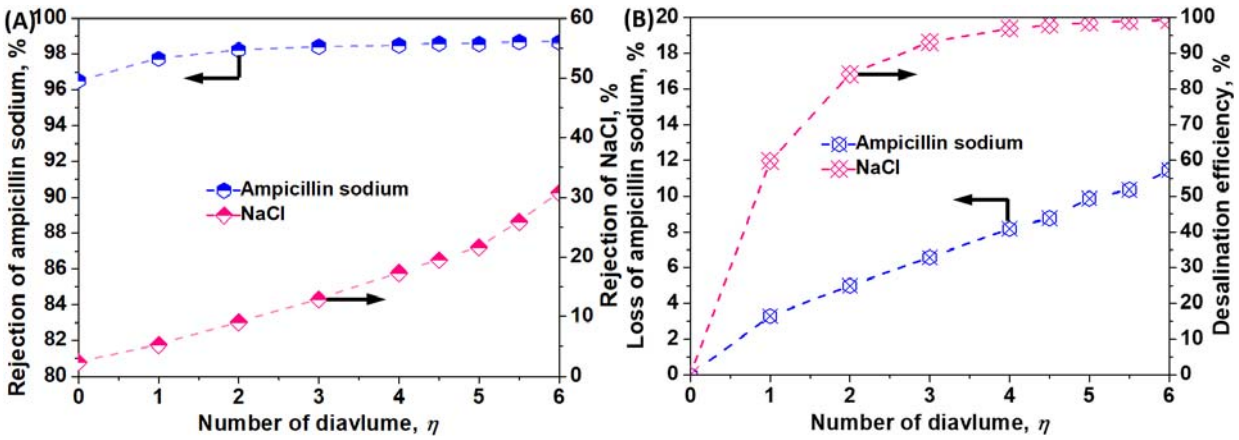

Fig. S14. Pressure-driven constant-volume nanofiltration-diafiltration performance of the NPM-6 membrane for fractionation of ampicillin sodium and NaCl from the ampicillin sodium/NaCl mixed solution. (**A**) Rejection of ampicillin sodium and NaCl and (**B**) loss of ampicillin sodium and desalination efficiency.

2.4 Desalination of pure NaCl solutions via electro-driven separation

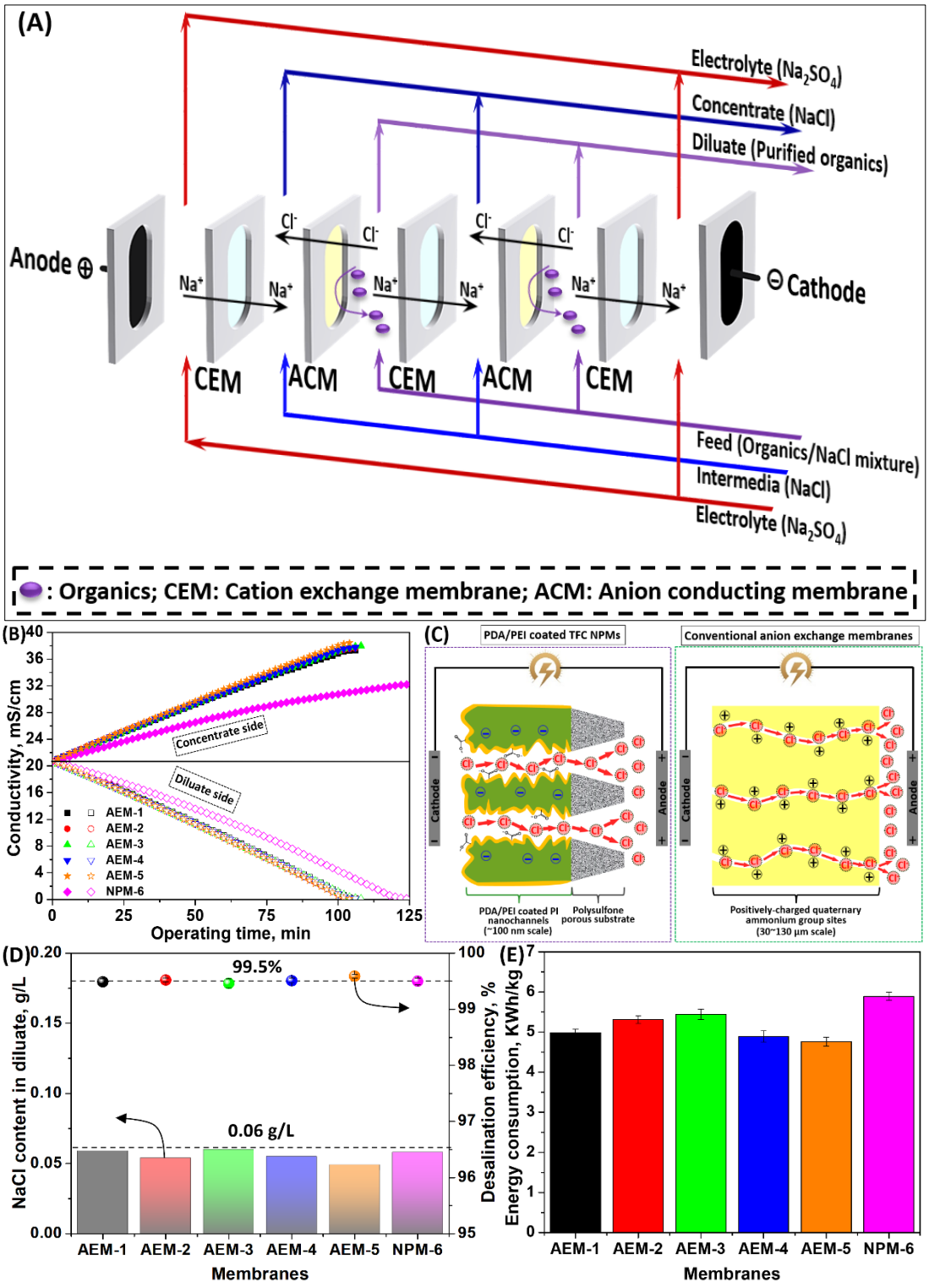

Fig. S15. Electrodialysis performance using commercial AEMs and NPM-6 membrane as anion conducting membranes. (**A**) Schematic of electrodialysis process for desalination, (**B**)

Conductivity profile in the concentrate and diluate as a function of operating time, (**C**) illustration of anion transfer pathway in the PDA/PEI-coated TFC NPMs and AEMs under an electric field, (**D**) NaCl content in the diluate and corresponding desalination efficiency, and (**E**) energy consumption.

Fig. S15 shows the electrodialysis performance of commercial AEMs and the PDA/PEI-coated TFC NPMs (i.e. NPM-6) for desalination of a pure NaCl solution (about 12 $g \cdot L^{-1}$). As shown in **Fig. S15B**, commercial AEMs exhibit faster anion transfer than the PDA/PEI-coated TFC NPMs (i.e., NPM-6), as reflected from the decay rate in the conductivity of the diluate. This is due to the positively-charged quaternary ammonium group sites carried by conventional AEMs, enabling faster anion transfer under the electric field, unlike the PDA/PEI-coated TFC NPMs, which are slightly negatively charged. However, the longer and more narrow ion diffusion pathway (30-130 micrometers thickness) of conventional AEMs can impede the ion transfer to some extent, while the PDA/PEI-coated NPMs (i.e., NPM-6) possess sufficient nano-channels with a thin selective layer (~100 nm thickness, **Fig. S15C**) that facilitates the anion transfer. Our investigation shows that both a surface charge effect and the physical structure of the ACMs seem to play important roles in efficient anion transfer capacity, which ultimately affect the desalination efficiency and energy consumption. Therefore, our results reflect that the PDA/PEI-coated TFC NPMs (which possess advantageous structural features) exhibit comparable desalination performances along with desalination efficiency and energy consumption to conventional AEMs (which possess advantageous surface charge features) when treating pure saline solution (**Figs. S15D** and **S15E**).

2.5 Electrodialytic fractionation of the antibiotic/NaCl mixed solutions using the PDA/PEI-coated TFC NPMs (NPM-6) as ACMs

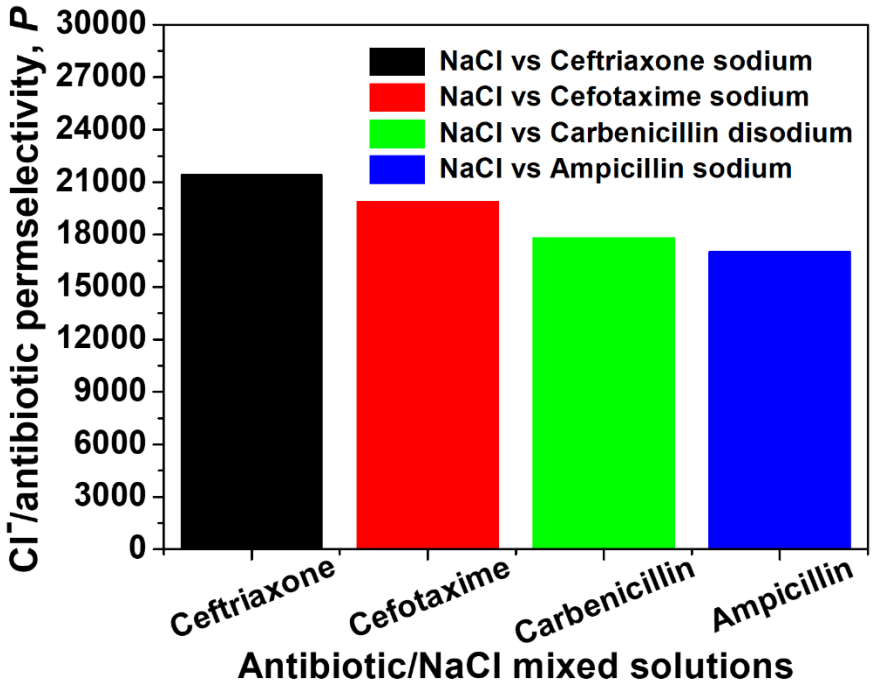

Fig. S16. The permselectivity between NaCl and antibiotics for NPM-6 during the electrocatalytic separation process

2.6 Electrodialytic fractionation of humic acid/NaCl mixed solution using the PDA/PEI-coated TFC NPMs (NPM-6) as ACMs

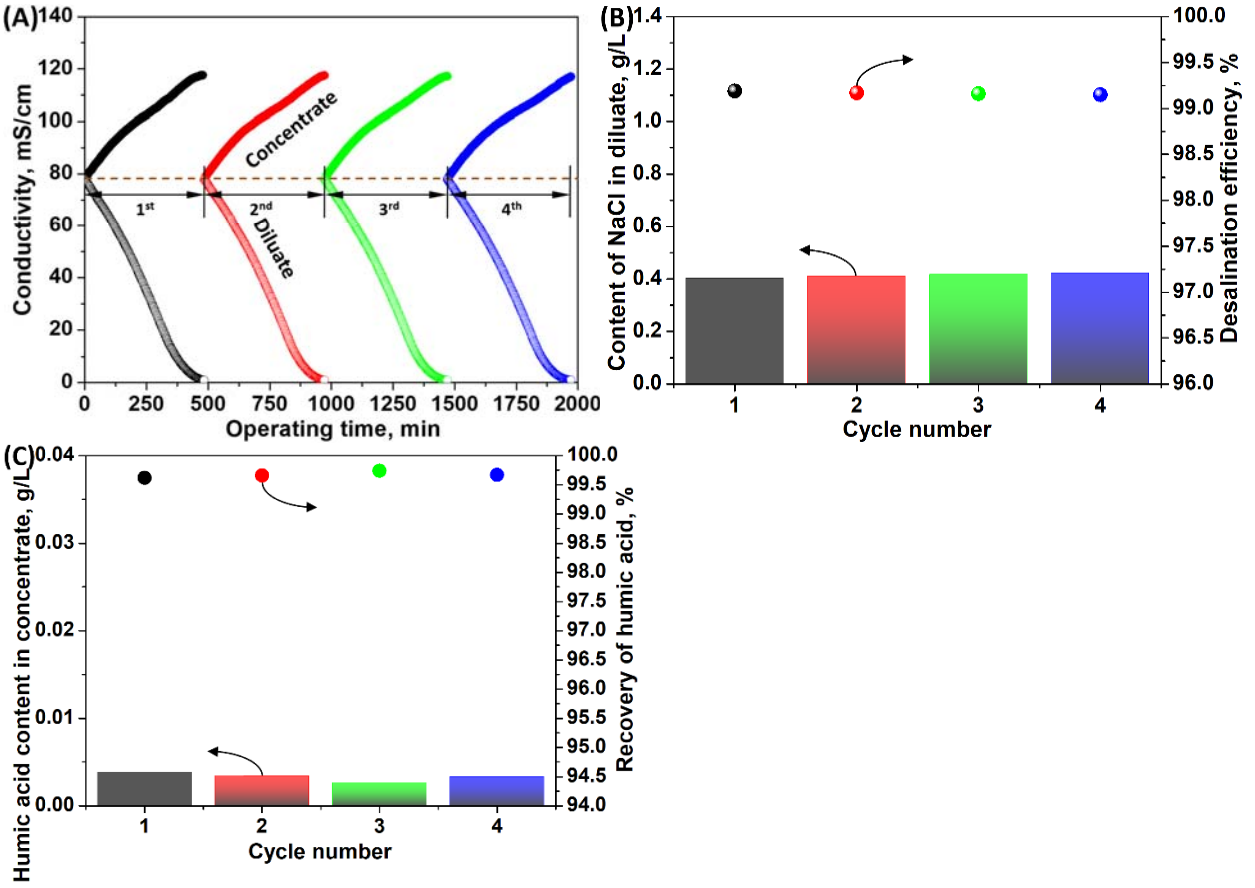

Fig. S17. Four-cycle electrodialytic separation process using the NPM-6 membrane as ACM for fractionation of the humic acid/NaCl mixed solution (salinity: ~50 g·L^{-1} NaCl). (**A**) Conductivity profile in the concentrate and diluate as a function of operating time, (**B**) content of NaCl in the diluate and corresponding desalination efficiency, (**C**) concentration of humic acid in the concentrate and its recovery rate.

In order to further verify the fractionation performance of the PDA/PEI-coated TFC NPMs in the organics/NaCl mixed solution with an elevated salinity, a four-cycle electrodialytic separation operation using the NPM-6 membrane as ACMs was conducted using the humic acid/NaCl mixed solution with a ~50 g·L^{-1} NaCl concentration as feed (**Fig. S17**).

As illustrated in **Fig. S17A**, the NPM-6 membrane also showed a nearly identical conductivity profile of the concentrate and diluate in the four-cycle electrodialytic separation operation in the humic acid/NaCl mixed solution with an elevated salinity (~50 g·L^{-1} NaCl), demonstrating an exceptional fouling resistance against humic acid. Moreover, the NPM-6 membrane manifested an impressive fractionation of humic acid and NaCl in the humic acid/NaCl mixed solution with a desalination efficiency of 99.2% (**Fig. S17B**) and humic acid recovery of over 99.6% (**Fig. S17C**). Such an extremely high retention of humic acid by the NPM-6 membrane during the electrodialytic

separation operation is driven by the synergistic effect of size exclusion and electrostatic repulsion, which is similar with the case that occurs in fractionation of antibiotic and NaCl.

2.7 Electrodialytic fractionation of organics/NaCl mixed solution using commercial AEM

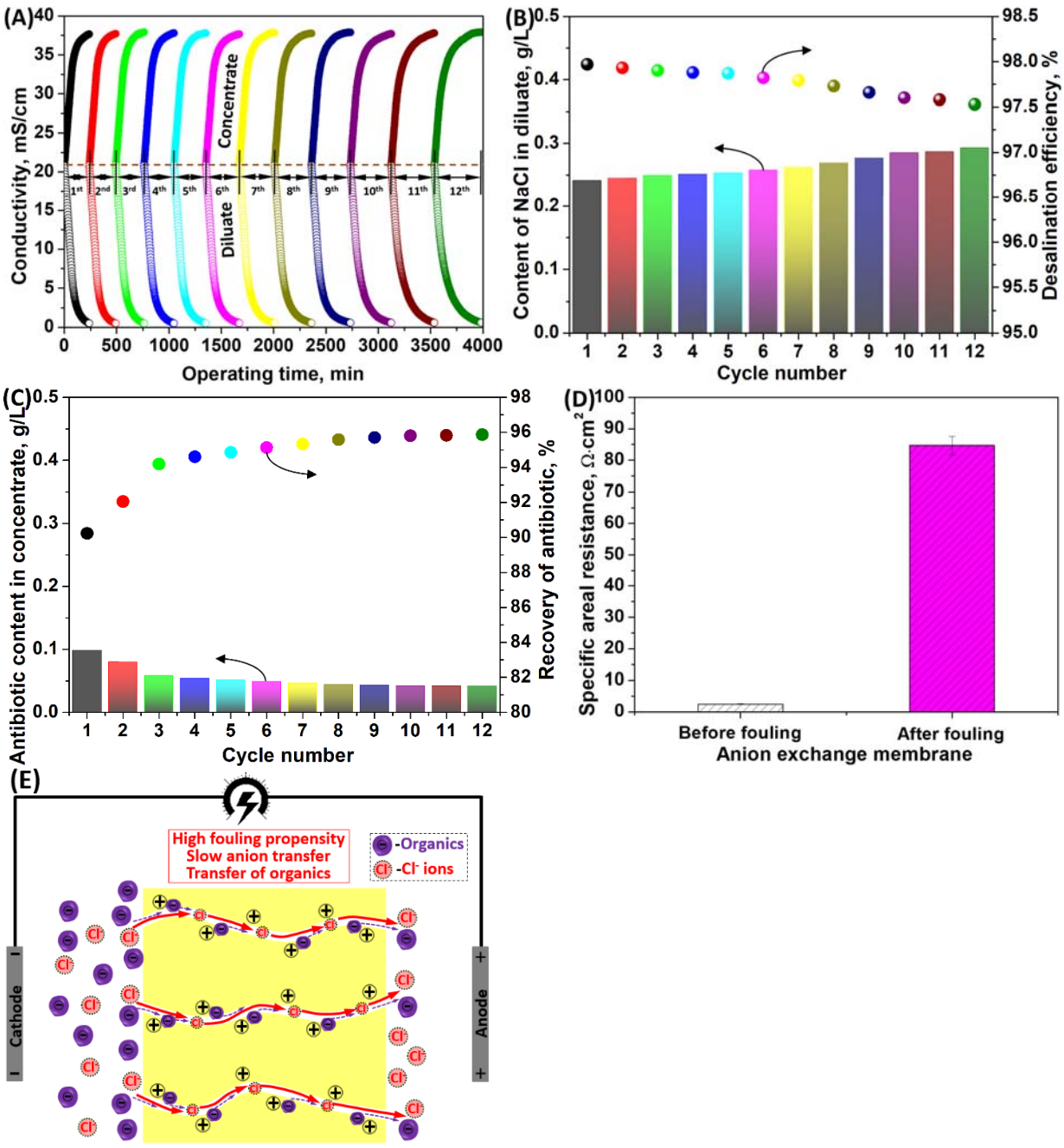

Fig. S18. Twelve-cycle electrodialysis process using commercial anion exchange membrane (AEM-5) during fractionation of ceftriaxone sodium/NaCl mixed solution (salinity: ~12 g·L^{-1} NaCl). (**A**) Conductivity profile in the concentrate and diluate as a function of operating time, (**B**) content of NaCl in diluate and corresponding desalination efficiency, (**C**) content of ceftriaxone sodium in concentrate and its recovery rate, (**D**) specific areal electric resistance of AEM-5 membrane before and after fouling, (**E**) schematics of anion (Cl^- and ceftriaxone ions) transfer of AEM-5 membrane during electrodialytic fractionation of ceftriaxone sodium and NaCl.

Membrane fouling is a critical aspect to evaluate the practical use of ACMs for one-step fractionation of organics and NaCl. To highlight the superiority of the surface-engineered PDA/PEI-coated NPMs in anion transfer for fractionation of the organics and NaCl, a traditional electrodialysis procedure equipped with commercial AEMs (i.e., AEM-5) was conducted using the ceftriaxone sodium/NaCl mixed solution as feed (**Fig. S18**).

As indicated in **Fig. S18A**, the commercial AEM (i.e., AEM-5) showed severer fouling, which was mainly attributed to the electrostatic attraction between the negatively-charged organics with a positively-charged AEM. This can significantly reduce the positive charge density of the AEM by the fouling process (as reflected by a boost in the specific areal electric resistance of the AEM-5 membrane by 33.0 times after fouling in **Fig. S18D**), thus impeding effective anion transfer (**Fig. S18E**). The fouling of the commercial AEM (AEM-1) requires increased system operation duration to remove the inorganic salt (i.e., NaCl) from the feed (i.e., diluate) for each cycle. Consequently, the membrane fouling deteriorates the desalination efficiency. The desalination efficiency of the commercial AEM (AEM-5) decreased from 98.0% to 97.5% when the ceftriaxone sodium/NaCl mixed solution was used as a feed solution in the six-cycle electrodialysis separation operation. Correspondingly, the content of NaCl in the ceftriaxone sodium/NaCl mixed solution was maintained at a level around 0.24 $g \cdot L^{-1}$ for the twelve-cycle electro-driven operation (**Fig. S18B**). On the other hand, the negatively-charged ceftriaxone ions inevitably transferred through the AEM-5 to the concentrate side through electrostatic attraction under the electric field, resulting in a high content of ceftriaxone (>41 $mg \cdot L^{-1}$) in the concentrate side and a low antibiotic recovery (<95.9%) (**Fig. S18C**). As demonstrated by the results in **Fig. 4**, the surface-engineered PDA/PEI-coated TFC NPM (NPM-6) as ACMs exhibited extraordinary antifouling properties, significantly outperforming the commercial AEMs for one-step fractionation of organics and inorganic salts during the electrodialytic separation process.

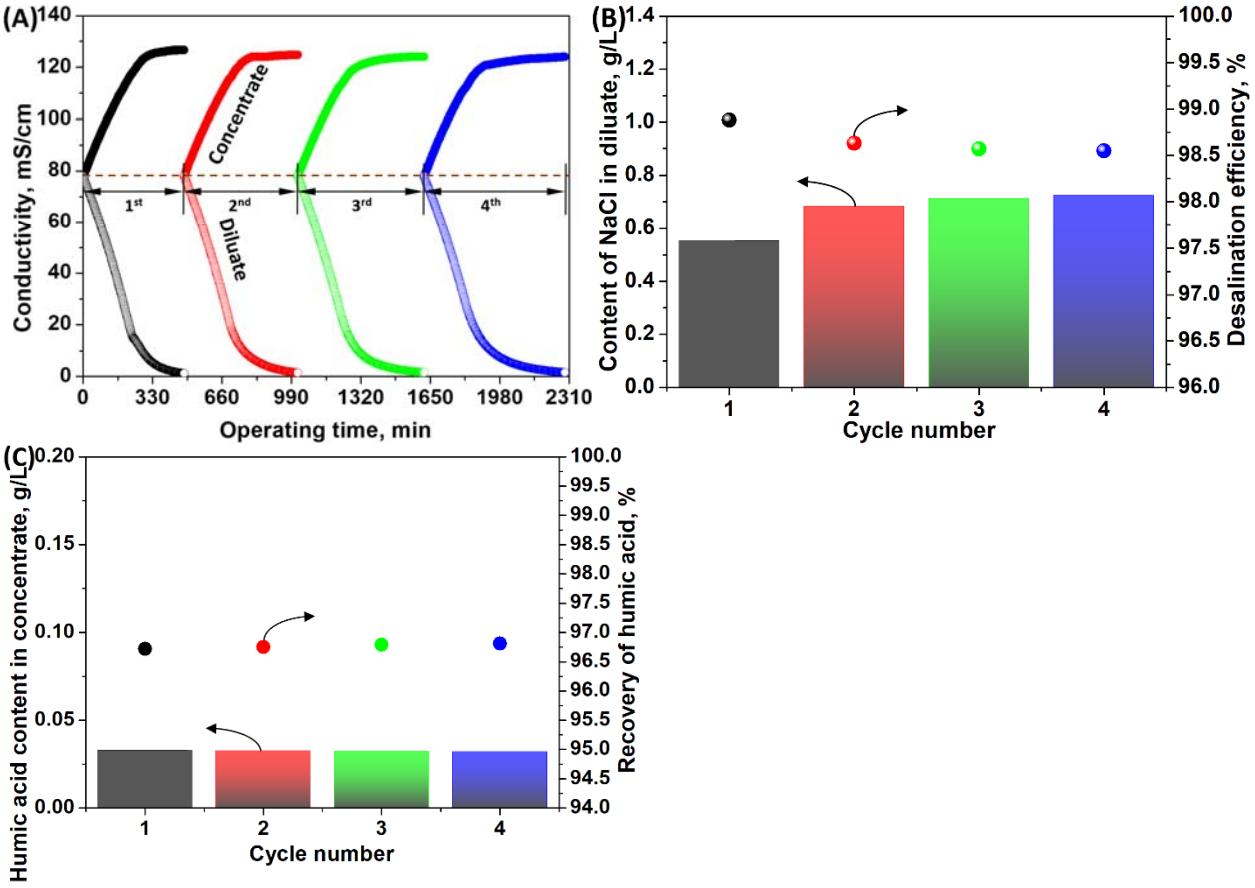

Fig. S19. Four-cycle electrodialysis process using the commercial AEM (AEM-5) during fractionation of the humic acid/NaCl mixed solution (salinity: ~50 g·L^{-1} NaCl). (**A**) Conductivity profile in the concentrate and diluate as a function of operating time, (**B**) content of NaCl in diluate and corresponding desalination efficiency, (**C**) content of humic acid in the concentrate and its recovery rate.

Table S1. Properties of commercial AEMs used for electrodialysis

Membrane (Brand)	Thickness (μm)	Ion exchange capacity ($meq \cdot g^{-1}$)	Specific areal electric resistance ($\Omega \cdot cm^2$)[a]	Selectivity (%)
AEM-1 (AEM-N1)	90	1.04	2.65±0.09	95-98
AEM-2 (TWEDA1R70)	90	1.26	1.98±0.12	>98
AEM-3 (FAS-30)	30	1.47	1.25±0.08	94-97
AEM-4 (FAS-PET-130)	130	0.94	3.46±0.16	92-97
AEM-5 (Neosepta@AMX)	140	1.57	2.49±0.16	98

[a] Specific areal electric resistance: Measured in a standard 0.5 $mol \cdot L^{-1}$ NaCl solution at 25 °C.

Table S2. XPS elemental composition analysis of the PDA/PEI-coated NPMs

Nanoporous membranes	C (at.%)	O (at.%)	N (at.%)
NPM-0 (Pristine)	78.2	15.3	6.5
NPM-1	73.2	15.5	11.3
NPM-2	72.3	16.2	11.5
NPM-3	72.1	15.9	12.0
NPM-4	71.8	15.9	12.3
NPM-5	71.8	15.7	12.5
NPM-6	71.9	15.5	12.6

Table S3. MWCO and effective mean pore sizes of the coated TFC NPMs

Nanoporous membranes	MWCO (Da)	μ_p (nm)
NPM-0 (Pristine)	682±17	0.48
NPM-1	603±21	0.44
NPM-2	526±16	0.40
NPM-3	446±17	0.39
NPM-4	378±14	0.38
NPM-5	346±12	0.38
NPM-6	325±11	0.38

Table S4. Membrane performance overview of the pressure-driven diafiltration performance for fractionation of organics and NaCl using the NPM-6 membrane

Organics/NaCl mixed solution	NaCl content in feed, $g \cdot L^{-1}$	Desalination efficiency,%	Recovery of organics,%
Ceftriaxone sodium/NaCl	0.078	99.34	95.82
Cefotaxime sodium/NaCl	0.075	99.37	93.73
Carbenicillin disodium/NaCl	0.077	99.35	91.02
Ampicillin sodium/NaCl	0.082	99.30	88.53

2.7 Movie captions

Movie S1. Transfer of Cl^- ions under an applied electric field of 1×10^{-2} V/Å.

Movie S2. Transfer of Na^+ ions under an applied electric field of 1×10^{-2} V/Å.

Movie S3. Transfer of ampicillin ions under the equilibrium state (without electric field) and an applied electric field of 1×10^{-2} V/Å.

References

1. C. Jiang, L. Zhang, P. Li, H. Sun, Y. Hou, Q. J. Niu, Ultrathin film composite membranes fabricated by novel in situ free interfacial polymerization for desalination. *ACS Appl. Mater. Inter.* **12**, 25304-25315 (2020).
2. J. Tian, H. Chang, S. Gao, Y. Zong, B. Van der Bruggen, R. Zhang, Direct generation of an ultrathin (8.5 nm) polyamide film with ultrahigh water permeance via in-situ interfacial polymerization on commercial substrate membrane. *J. Membr. Sci.* **634**, 119450 (2021).
3. M. I. Khan, A. N. Mondal, B. Tong, C. Jiang, K. Emmanuel, Z. Yang, L. Wu, T. Xu, Development of BPPO-based anion exchange membranes for electrodialysis desalination applications. *Desalination* **391**, 61-68 (2016).
4. Y. Zhao, Y. Li, S. Yuan, J. Zhu, S. Houtmeyers, J. Li, R. Dewil, C. Gao, B. Van der Bruggen, A chemically assembled anion exchange membrane surface for monovalent anion selectivity and fouling reduction. *J. Mater. Chem. A* **7**, 6348-6356 (2019).
5. X. Kong, M. Zhou, C. Lin, J. Wang, B. Zhao, X. Wei, B. Zhu, Polyamide/PVC based composite hollow fiber nanofiltration membranes: Effect of substrate on properties and performance. *J. Membr. Sci.* **505**, 231-240 (2016).
6. J. Lin, Q. Chen, R. Liu, W. Ye, P. Luis, B. Van der Bruggen, S. Zhao, Sustainable management of landfill leachate concentrate via nanofiltration enhanced by one-step rapid assembly of metal-organic coordination complexes. *Water Res.* **204**, 117633 (2021).
7. J. Gao, S. Sun, W. Zhu, T. Chung, Polyethyleneimine (PEI) cross-linked P84 nanofiltration (NF) hollow fiber membranes for Pb2+ removal. *J. Membr. Sci.* **452**, 300-310 (2014).
8. L. Shao, X. Q. Cheng, Y. Liu, S. Quan, J. Ma, S. Z. Zhao, K. Y. Wang, Newly developed nanofiltration (NF) composite membranes by interfacial polymerization for Safranin O and Aniline blue removal. *J. Membr. Sci.* **430**, 96-105 (2013).
9. National center for biotechnology information, PubChem compound summary for CID 44145008 (available at https://pubchem.ncbi.nlm.nih.gov/compound/44145008).
10. National center for biotechnology information, PubChem compound summary for CID 681, Dopamine (available at https://pubchem.ncbi.nlm.nih.gov/compound/Dopamine).
11. N. M. O'Boyle, M. Banck, C. A. James, C. Morley, T. Vandermeersch, G. R. Hutchison, Open Babel: An open chemical toolbox. *J. Cheminformatics* **3**, 33 (2011).
12. Ampicillin sodium salt, $C_{16}H_{18}N_3NaO_4S$ - PubChem (available at https://pubchem.ncbi.nlm.nih.gov/compound/Ampicillin_-Sodium-Salt).
13. A. I. Jewett, D. Stelter, J. Lambert, S. M. Saladi, O. M. Roscioni, M. Ricci, L. Autin, M. Maritan, S. M. Bashusqeh, T. Keyes, R. T. Dame, J. Shea, G. J. Jensen, D. S. Goodsell, Moltemplate: A tool for Coarse-Grained modeling of complex biological matter and soft condensed matter physics. *J. Mol. Biol.* **433**, 166841 (2021).
14. J. Wang, R. M. Wolf, J. W. Caldwell, P. A. Kollman, D. A. Case, Development and testing of a general amber force field. *J. Comput. Chem.* **25**, 1157-1174 (2004).
15. D. J. Price, C. L. Brooks, A modified TIP3P water potential for simulation with Ewald summation. *J. Chem. Phys.* **121**, 10096-10103 (2004).
16. I. S. Joung, T. E. Cheatham, Determination of alkali and halide monovalent ion parameters for use in explicitly solvated biomolecular simulations. *J. Phys. Chem. B* **112**, 9020-9041 (2008).
17. A. P. Thompson, H. M. Aktulga, R. Berger, D. S. Bolintineanu, W. M. Brown, P. S. Crozier, P. J. In T Veld, A. Kohlmeyer, S. G. Moore, T. D. Nguyen, R. Shan, M. J. Stevens, J. Tranchida, C. Trott, S. J. Plimpton, LAMMPS - a flexible simulation tool for particle-based materials

modeling at the atomic, meso, and continuum scales. *Comput. Phys. Commun.* **271**, 108171 (2022).
18. W. Humphrey, A. Dalke, K. Schulten, VMD: Visual molecular dynamics. *J. Mol. Graph.* **14**, 33-38 (1996).
19. D. H. Seo, S. Pineda, Y. C. Woo, M. Xie, A. T. Murdock, E. Y. M. Ang, Y. Jiao, M. J. Park, S. I. Lim, M. Lawn, F. F. Borghi, Z. J. Han, S. Gray, G. Millar, A. Du, H. K. Shon, T. Y. Ng, K. K. Ostrikov, Anti-fouling graphene-based membranes for effective water desalination. *Nat. Commun.* **9**, 683 (2018).
20. D. Cohen-Tanugi, J. C. Grossman, Water desalination across nanoporous graphene. *Nano Lett.* **12**, 3602-3608 (2012).
21. M. Liu, J. Ji, X. Zhang, X. Zhang, B. Yang, F. Deng, Z. Li, K. Wang, Y. Yang, Y. Wei, Self-polymerization of dopamine and polyethyleneimine: Novel fluorescent organic nanoprobes for biological imaging applications. *J. Mater. Chem. B* **3**, 3476-3482 (2015).
22. W. Qiu, H. Yang, Z. Xu, Dopamine-assisted co-deposition: An emerging and promising strategy for surface modification. *Adv. Colloid Interfaces Sci.* **256**, 111-125 (2018).
23. C. Zhao, F. Zuo, Z. Liao, Z. Qin, S. Du, Z. Zhao, Mussel-inspired one-pot synthesis of a fluorescent and water-soluble polydopamine-polyethyleneimine copolymer. *Macromol. Rapid Comm.* **36**, 909-915 (2015).
24. J. Wang, K. Ren, H. Chang, S. Zhang, L. Jin, J. Ji, Facile fabrication of robust superhydrophobic multilayered film based on bioinspired poly(dopamine)-modified carbon nanotubes. *Phys. Chem. Chem. Phys.* **16**, 2936-2943 (2014).